




Quantitative proteomics in medication-related osteonecrosis of the jaw: A proof-of-concept study

Alejandro I. Lorenzo-Pouso¹  | Susana B. Bravo² | Javier Carballo³ |
 María del Pilar Chantada-Vázquez² | José Bagán⁴ | Leticia Bagán⁴ |
 Cintia M. Chamorro-Petronacci¹  | Mercedes Conde-Amboage⁵ |
 Rafael López-López⁶ | Abel García-García¹ | Mario Pérez-Sayáns¹ 

¹Oral Medicine, Oral Surgery and Implantology Unit, MedOralRes Group, University of Santiago de Compostela, Health Research Institute of Santiago de Compostela (IDIS), Santiago de Compostela, Spain

²Proteomic Unit, Health Research Institute of Santiago de Compostela (IDIS), University Clinical Hospital of Santiago de Compostela, Santiago de Compostela, Spain

³Department of Food Technology, Faculty of Sciences, University of Vigo-Ourense Campus, Vigo, Spain

⁴Department of Stomatology and Maxillofacial Surgery, University General Hospital of Valencia, Valencia, Spain

⁵Models of Optimization, Decision, Statistics and Applications Research Group (MODESTYA). Department of Statistics, Mathematical Analysis and Optimization, University of Santiago de Compostela, Santiago de Compostela, Spain

⁶Translational Medical Oncology Group (Oncomet), Health Research Institute of Santiago (IDIS), University Hospital Complex of Santiago de Compostela (SERGAS), Santiago de Compostela, Spain

Correspondence

Alejandro I. Lorenzo-Pouso, Oral Medicine, Oral Surgery and Implantology Unit, MedOralRes Group, University of Santiago de Compostela, Health Research Institute of Santiago de Compostela (IDIS), Entrerriós s/n; Santiago de Compostela, 15782, A Coruña, Spain.
 Email: alejandrismael.lorenzo@rai.usc.es

Abstract

Objective: Medication-related osteonecrosis of the jaw (MRONJ) is a paradoxical effect associated with bone-modifying agents (BMAs) and other drugs. Currently, no valuable diagnostic or prognosis biomarkers exist. The goal of this research was to study MRONJ-related salivary proteome.

Materials and Methods: This case-control aimed to study salivary proteome in MRONJ versus control groups (i) formed from BMAs consumers and (ii) healthy individuals to unravel biomarkers. Thirty-eight samples of unstimulated whole saliva (18 MRONJ patients, 10 BMA consumers, and 10 healthy controls) were collected. Proteomic analysis by SWATH-MS coupled with bioinformatics analysis was executed.

Results: A total of 586 proteins were identified, 175 proteins showed significant differences among MRONJ versus controls. SWATH-MS revealed differentially expressed proteins among three groups, which have never been isolated. These proteins had distinct roles including cell envelope organization, positive regulation of vesicle fusion, positive regulation of receptor binding, or regulation of low-density lipoprotein particle clearance. Integrative analysis prioritized 3 proteins (MMP9, AACT, and HBD). Under receiver-operating characteristic analysis, this panel discriminated MRONJ with a sensitivity of 90% and a specificity of 78.9%.

Conclusion: These findings may inform a novel biomarker panel for MRONJ prediction or diagnosis. Nonetheless, further research is needed to validate this panel.

KEYWORDS

biomarker discovery, MRONJ, prevention, prognosis, proteomics, saliva

1 | INTRODUCTION

Bone-modifying agents (BMAs) are used to decrease fracture risk as prevention and treatment for osteoporosis or bone metastasis among other diseases. BMAs control bone turnover and mineral density, microstructure, geometry, and material properties (Reid, 2015). Nonetheless, a paradoxical reaction of BMAs at the jaw has been described, namely medication-related osteonecrosis of the jaw (MRONJ) (Marx, 2003). According to the American Association of Oral and Maxillofacial Surgeons, MRONJ diagnosis is made in the presence of exposed bone or bone that can be probed through an intraoral or extraoral fistula in the maxillofacial region and that does not heal within 8 weeks and that occurs in a patient who has received a BMA or antiangiogenics and has no history of head and neck radiotherapy (Otto et al., 2018; Ruggiero et al., 2014). MRONJ etiology appears multifactorial, and many questions remain regarding prevention and management (Schioldt et al., 2019).

Nowadays, no validated clinical biomarkers exist to identify patients at risk of suffering from this BMA adverse event. Our group and others found several salivary biomarkers to be differently expressed in MRONJ (Bagan et al., 2013; Bagan, Saez, Tormos, Hens, et al., 2014; Bagan, Saez, Tormos, Gavalda-Esteve, et al., 2014; Thumbigere-Math et al., 2015). However, low-quality evidence supports the use of these biomarkers. Over the last years the application of proteomics, the large-scale high throughput analysis of proteins of an organism, has been expanded to the study of saliva with the goal of identifying biomarkers with diagnostic or prognostic value, particularly mass spectrometry is the most desirable approach for the study of the salivary proteome (Rifai et al., 2006). Recently, most advanced approaches have been used to quantify proteins in saliva using data-independent acquisition (DIA) by SWATH-MS (Rifai et al., 2006). Although previous data-dependent analysis (DDA) is necessary to generate a spectral library (Bateman et al., 2014).

Prompted by the literature discussed, this work aimed to search differently expressed MRONJ-related salivary proteins using SWATH-MS technology.

2 | MATERIAL AND METHODS

2.1 | Design

This research was elaborated as a case-control study. Group 1 was composed of MRONJ cases (Ruggiero et al., 2014). Group 2 was built of age-balanced and gender-matched individuals undergoing treatment with BMAs for more than 24 months without MRONJ clinical or radiographic evidence. Group 3 was based on healthy volunteers.

Cases were selected from Stomatology and Maxillofacial Surgery Unit at the University General Hospital of Valencia, Spain, and controls were enrolled from the Oncology Service of University Hospital Complex of Santiago de Compostela, Spain, between January 2018 and June 2019. Participants were comprehensively informed and signed consent before their inclusion, according to both local Ethical Committees (Reference: 301118). STROBE guidelines were followed in this study (von Elm et al., 2008). All procedures were performed according to 1964 Helsinki Declaration and its subsequent amendments.

2.2 | Clinical data

Patient's medical records with BMA type, dose, treatment duration, and base disease were gathered. Two dental practitioners conducted an intraoral examination of patients recording: location and staging of MRONJ and the presence of infection or pain. In addition, other oral measures were recorded: DMF index, supragingival plaque index, gingival inflammation, depth of periodontal pockets in Ramfjord teeth, and clinical attachment level. Interexaminer agreement was checked by means of intraclass correlation coefficients

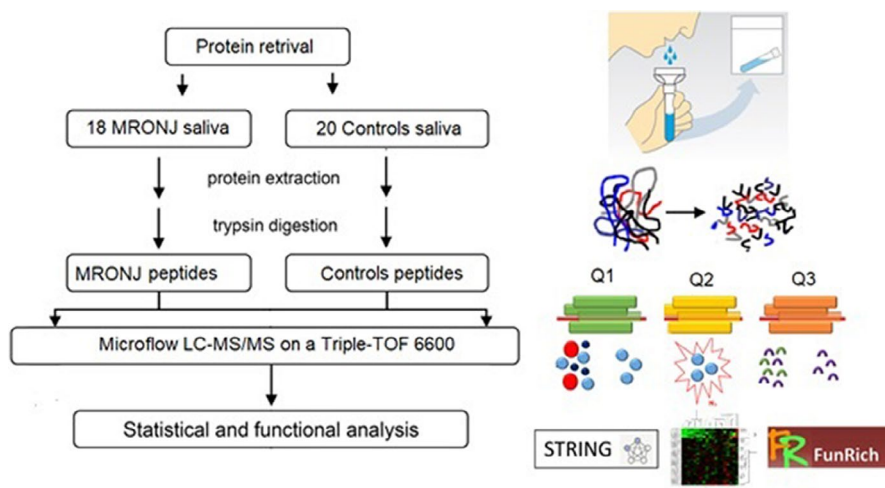


FIGURE 1 Workflow of the protein identification and quantification by the use of SWATH-MS analysis

(ICCs). Intraexaminer pooled ICC for all dental indices was 0.82 (95%CI 0.81-0.84). Interexaminer weighted ICC value for these variables was 0.79 (95%CI 0.72-0.87).

2.3 | Saliva sampling and storage

Unstimulated whole saliva (5 ml) was collected by having each participant swallow and expectorate saliva into a 20 ml sterile polypropylene tube for 5–10 min. To reduce proteome variations related to food intake or circadian variation all salivary samples were taken in the early morning and at least two hours after food intake. Blood contamination was also avoided. For this purpose, subjects were asked to refrain from brushing their teeth within an hour prior to sample collection. After this process, samples were centrifuged (20 min at 2000×g) to disaggregate cells/debris. Resulting supernatant was aliquoted into 1 ml tubes and mixed with a protease inhibitor cocktail (Halt, ThermoFisher Scientific, MA, US).

Samples were preserved at -80°C in the biorepository established at the Proteomic Unit until analysis. [Figure 1](#) depicts workflow.

2.4 | Protein in-gel digestion

Protein concentration was determined by a colorimetric assay (RC-DC, Biorad, CA, USA). An equal amount of protein, particularly 100 μg from all samples, was loaded on 10% SDS-PAGE gel. Electrophoresis was performed until BPB reached the top of the gel concentrating proteins in a gel single band. Bands were visualized by sypro staining, excised, and cut into fragments to be washed successively with water purified with a Millipore system and 50 mM ammonium bicarbonate dissolved in 50% methyl alcohol. Resulting gel fragments were subjected to dehydration with acetonitrile in a vacuum centrifuge. Protein samples were reduced with 10 mM dithiothreitol dissolved in 50 mM ammonium bicarbonate at 60°C for 30 min. Secondly to this process, samples were subjected to alkylation with 55 mM iodoacetamide dissolved in 50 mM ammonium bicarbonate at a temperature of 20°C for a period of 30 min. The final mix was digested with a solution of 20 ng/ μl trypsin in 20 mM ammonium bicarbonate incubating at 37°C for 16 h. Lastly, resulting peptides were dissolved in a solution composed of 0.1% formic acid.

2.5 | SWATH library creation and relative protein quantification

DDA/DIA analyses were conducted essentially as explained in a previous report (Chantada-Vazquez et al., 2020). Samples from each group were pooled with equal aliquots. The peptide solutions were processed with shotgun DDA by micro-flow LC-MS/MS. Briefly, the analytical column was a Chrom XP C18 column with a 3 mm particle size and 120 \AA pore size (Eksigent, Sciex Redwood City, CA, USA). Analytical precolumn was a TriartC18 column (YMC CO., LTD.,

Japan) with a flow rate of 5 $\mu\text{l}/\text{min}$. The micro-pump was operated under gradient elution conditions using two mobile phases: (i) 0.1% formic acid in purified water and (ii) 0.1% formic acid in acetonitrile.

A quadrupole-TOF mass spectrometer (i.e., Triple TOF 6600 [SCIEX, Framingham, MA, USA]) working in ESI+performed DDA analysis. Mass spectrometry analysis parameters were ion spray voltage at 2300 V, curtain gas at 35.0, ion source gas 1 at 15.0, ion source gas 2 at 0.0, interface heater temperature at 150°C , and entrance potential at 10.0. Analysis was controlled with the Analyst TF 1.7.1 Software (Sciex, Redwood City, CA, USA). For proteome identification Protein Pilot software (v.5.0.1. Sciex) with a human-specific dataset was used.

Samples were analyzed using the DIA approach to reach a relative quantification. 4 μl of each sample was processed using the LC-MS and LC gradient for building the spectral library. The method to obtain a relative quantification consisted of repeating cycles. Each cycle was made by the acquisition of 65 TOF MS/MS scans (400 to 1500 m/z , high sensitivity mode, 50 ms acquisition time) of intersecting sequential precursor isolation windows of variable width (1 m/z overlap) covering the 400 to 1250 m/z mass range with a previous TOF MS scan for each cycle. Total cycle time for each run lasted 6.3 s. Variability in terms of width was optimized according to the ion density determined by DDA runs.

2.6 | Statistical analysis

Continuous normally distributed variables certified with the Kolmogorov–Smirnov test were expressed as mean \pm standard deviation. While categorical variables were reported with percentages. On this basis, quantitative variables in multiple independent samples were studied using the Student's *t*-test or the Mann–Whitney U and Kruskal–Wallis test on the basis of the Gaussian or non-Gaussian distributions.

Peak extraction was performed using the SWATH Acquisition 2.0 MicroApp (Sciex, Framingham, MA, USA). Peptides with a confidence score above 99% were included in DDA spectral library. False discovery rate was calculated for each peptide, and 1% was used as the cut-off point for inclusion. The fold changes (FCs) in protein expression were defined as median ratios of spectra significantly matched to each protein with signals reported across all samples. Proteins that in the quantification displayed $p < .05$ and with a FC ratio >2 were considered for analysis. In protein quantification, significant differences between comparisons were done by principal component analysis (PCA) and orthogonal partial least squares discriminant analysis (OPLS-DA). The method chosen for model selection was the Akaike information criterion to avoid collinearity effects.

2.7 | Bioinformatic analysis

Functional analysis was performed by FunRich (Functional Enrichment analysis tool). In addition, Search Tool for the Retrieval of Interacting Genes/Proteins (STRINGS) was used for the analysis of protein-protein

TABLE 1 List of altered proteins in medication-related osteonecrosis of the jaw patients (Group 1) versus both control groups taking bone-modifying agents (Group 2) and not (Group 3)

Accession number	Protein description	Protein symbol	Fold change	p value ^a
P04280	PRP1	Basic salivary proline-rich protein 1	↑5.95	0.0503
P02763	A1AG1	Alpha-1-acid glycoprotein 1	↑5.40	0.0001
P00738	HPT	Haptoglobin	↑4.98	4.29E-06
P01009	A1AT	Alpha-1-antitrypsin	↑4.19	3.19E-05
P02790	HEMO	Hemopexin	↑3.76	0.0002
P68871	HBB	Hemoglobin subunit beta	↑3.27	0.0099
O75594	PGRP1	Peptidoglycan recognition protein 1	↑3.25	8.35E-09
P01008	ANT3	Antithrombin-III	↑3.25	4.04E-05
P69905	HBA	Hemoglobin subunit alpha	↑3.20	0.0124
P02042	HBD	Hemoglobin subunit delta	↑3.16	0.0024
P04217	A1BG	Alpha-1B-glycoprotein	↑2.98	2.47E-05
P01011	AACT	Alpha-1-antichymotrypsin	↑2.89	0.0007
P01857	IGHG1	Immunoglobulin heavy constant gamma 1	↑2.79	0.0002
P01877	IGHA2	Immunoglobulin heavy constant alpha 2	↑2.77	0.0020
P02760	AMBP	Protein AMBP	↑2.76	0.0001
P02749	APOH	Beta-2-glycoprotein 1	↑2.73	0.0001
P80748	LV321	Immunoglobulin lambda variable 3-21	↑2.73	0.0001
P02750	A2GL	Leucine-rich alpha-2-glycoprotein	↑2.72	0.0036
P04114	APOB	Apolipoprotein B-100	↑2.72	0.0005
P01859	IGHG2	Immunoglobulin heavy constant gamma 2	↑2.65	0.0009
P01834	IGKC	Immunoglobulin kappa constant	↑2.61	1.33E-05
P00915	CAH1	Carbonic anhydrase 1	↑2.57	0.0133
P00450	CERU	Ceruloplasmin	↑2.57	0.0003
P01023	A2MG	Alpha-2-macroglobulin	↑2.51	0.0007
P01594	KV133	Immunoglobulin kappa variable 1-33	↑2.50	0.0001
P01782	HV309	Immunoglobulin heavy variable 3-9	↑2.49	0.0636
P02787	TRFE	Serotransferrin	↑2.48	0.0074
P05546	HEP2	Heparin cofactor 2	↑2.46	0.0019
A0A0C4DH68	KV224	Immunoglobulin kappa variable 2-24	↑2.45	0.0134
P02768	ALBU	Serum albumin	↑2.45	0.0024
P01024	CO3	Complement C3	↑2.44	0.0023
Q14624	ITIH4	Inter-alpha-trypsin inhibitor heavy chain H4	↑2.39	0.0003
P02766	TTHY	Transthyretin	↑2.36	4.78E-05
P01611	KVD12	Immunoglobulin kappa variable 1D-12	↑2.35	0.0002
P02812	PRB2	Basic salivary proline-rich protein 2	↑2.34	0.0872
P01700	LV147	Immunoglobulin lambda variable 1-47	↑2.32	0.0046
P22894	MMP8	Neutrophil collagenase	↑2.31	3.78E-06
P05155	IC1	Plasma protease C1 inhibitor	↑2.24	0.0016
A0A0B4J1X5	HV374	Immunoglobulin heavy variable 3-74	↑2.23	0.0162
P25311	ZA2G	Zinc-alpha-2-glycoprotein	↑2.23	0.0088
P80188	NGAL	Neutrophilgelatinase-associated lipocalin	↑2.22	2.02E-08
P01717	LV325	Immunoglobulin lambda variable 3-25	↑2.21	0.0023
O75015	FCG3B	Low-affinity immunoglobulin gamma Fc region receptor III-B	↑2.16	2.45E-05
P61769	B2MG	Beta-2-microglobulin	↑2.16	0.0007

TABLE 1 (Continued)

Accession number	Protein description	Protein symbol	Fold change	p value ^a
P0C0L5	CO4B	Complement C4-B	↑2.15	0.0018
P06870	KLK1	Kallikrein-1	↑2.12	0.0174
P01860	IGHG3	Immunoglobulin heavy constant gamma 3	↑2.09	0.0082
P04040	CATA	Catalase	↑2.03	2.33E-09
P02679	FIBG	Fibrinogen gamma chain	↑2.03	0.0175
Q04118	PRB3	Basic salivary proline-rich protein 3	↑2.02	0.0957
P14780	MMP9	Matrix metalloproteinase-9	↑2.01	0.0000
P09228	CYTT	Cystatin-SA	↑2.01	0.0639
P13646	K1C13	Keratin, type I cytoskeletal 13	↓18.12	2.60E-14
P02538	K2C6A	Keratin, type II cytoskeletal 6A	↓17.93	7.31E-10
Q9UBC9	SPRR3	Small proline-rich protein 3	↓13.14	0.0001
P08779	K1C16	Keratin, type I cytoskeletal 16	↓13.02	1.15E-12
Q01546	K22O	Keratin, type II cytoskeletal 2 oral	↓12.71	2.24E-12
P05387	RLA2	60S acidic ribosomal protein P2	↓12.24	1.04E-07
P19013	K2C4	Keratin, type II cytoskeletal 4	↓12.20	3.64E-15
P05787	K2C8	Keratin, type II cytoskeletal 8	↓12.10	1.25E-10
P04259	K2C6B	Keratin, type II cytoskeletal 6B	↓11.08	6.11E-11
P02533	K1C14	Keratin, type I cytoskeletal 14	↓10.54	5.20E-12
Q9HCY8	S10AE	Protein S100-A14	↓10.52	1.70E-08
P47929	LEG7	Galectin-7	↓9.60	6.06E-14
P12035	K2C3	Keratin, type II cytoskeletal 3	↓9.30	2.31E-06
P13647	K2C5	Keratin, type II cytoskeletal 5	↓9.30	1.33E-11
P04792	HSPB1	Heat shock protein beta-1	↓8.82	3.88E-14
Q8N1N4	K2C78	Keratin, type II cytoskeletal 78	↓8.78	3.64E-18
Q09666	AHNK	Neuroblast differentiation-associated protein AHNAK	↓8.50	5.32E-11
P46776	RL27A	60S ribosomal protein L27a	↓8.16	1.31E-16
Q99943	PLCA	1-acyl-sn-glycerol-3-phosphate acyltransferase alpha	↓8.11	0.0015
Q15231	ZN185	Zinc finger protein 185	↓7.65	8.37E-10
Q13835	PKP1	Plakophilin-1	↓7.05	2.65E-19
P15924	DESP	Desmoplakin	↓6.85	8.21E-18
Q96FQ6	S10AG	Protein S100-A16	↓6.77	1.55E-19
P07355	ANXA2	Annexin A2	↓6.63	2.36E-20
Q92817	EVPL	Envoplakin	↓6.47	2.28E-13
P60903	S10AA	Protein S100-A10	↓6.39	3.94E-20
P14923	PLAK	Junction plakoglobin	↓6.38	5.47E-17
P48668	K2C6C	Keratin, type II cytoskeletal 6C	↓6.35	9.12E-11
P36578	RL4	60S ribosomal protein L4	↓6.20	5.60E-15
Q04695	K1C17	Keratin, type I cytoskeletal 17	↓5.90	1.79E-12
P04083	ANXA1	Annexin A1	↓5.82	9.13E-21
P67936	TPM4	Tropomyosin alpha-4 chain	↓5.75	1.17E-06
Q02413	DSG1	Desmoglein-1	↓5.74	3.10E-14
P02511	CRYAB	Alpha-crystallin B chain	↓5.67	5.80E-09
P27482	CALL3	Calmodulin-like protein 3	↓5.61	1.84E-05
Q9UBG3	CRNN	Cornulin	↓5.32	3.14E-16

TABLE 1 (Continued)

Accession number	Protein description	Protein symbol	Fold change	p value ^a
P02545	LMNA	Prelamin-A/C	↓5.29	1.88E-17
P22735	TGM1	Protein-glutamine gamma-glutamyltransferase K	↓5.25	1.82E-11
P08727	K1C19	Keratin, type I cytoskeletal 19	↓5.24	7.94E-10
O60437	PEPL	Periplakin	↓5.20	1.48E-13
P21796	VDAC1	Voltage-dependent anion-selective channel protein 1	↓5.18	1.21E-15
P12236	ADT3	ADP/ATP translocase 3	↓5.08	1.17E-10
P46783	RS10	40S ribosomal protein S10	↓5.07	5.08E-15
Q8WVV4	POF1B	Protein POF1B	↓4.96	1.89E-15
Q9NZT1	CALL5	Calmodulin-like protein 5	↓4.92	0.0004
P10599	THIO	Thioredoxin	↓4.76	1.78E-16
P05386	RLA1	60S acidic ribosomal protein P1	↓4.62	4.76E-12
P29034	S10A2	Protein S100-A2	↓4.58	4.41E-18
P07476	INVO	Involucrin	↓4.54	2.78E-06
Q9NSB2	KRT84	Keratin, type II cuticular Hb4	↓4.38	6.97E-07
P62851	RS25	40S ribosomal protein S25	↓4.36	1.76E-13
B3EWG6	FM25G	Protein FAM25G	↓4.20	0.0007
P62249	RS16	40S ribosomal protein S16	↓4.20	7.71E-13
Q9GZV4	IF5A2	Eukaryotic translation initiation factor 5A-2	↓4.13	2.76E-15
O95171	SCEL	Sciellin	↓4.12	5.06E-11
Q99879	H2B1 M	Histone H2B type 1-M	↓3.97	4.61E-14
Q08188	TGM3	Protein-glutamine gamma-glutamyltransferase E	↓3.95	1.00E-14
P16401	H15	Histone H1.5	↓3.94	1.46E-07
Q5VTE0	EF1A3	Putative elongation factor 1-alpha-like 3	↓3.94	1.89E-14
P19012	K1C15	Keratin, type I cytoskeletal 15	↓3.88	1.11E-10
P08670	VIME	Vimentin	↓3.44	0.0004
P36952	SPB5	Serpin B5	↓3.34	5.66E-14
P13987	CD59	CD59 glycoprotein	↓3.33	1.29E-06
O95833	CLIC3	Chloride intracellular channel protein 3	↓3.32	4.94E-09
P62805	H4	Histone H4	↓3.28	2.21E-10
P13639	EF2	Elongation factor 2	↓3.27	3.42E-15
P68366	TBA4A	Tubulin alpha-4A chain	↓3.25	7.60E-15
P30050	RL12	60S ribosomal protein L12	↓3.25	1.16E-12
P68371	TBB4B	Tubulin beta-4B chain	↓3.23	2.00E-15
P31947	1433S	14-3-3 protein sigma	↓3.21	1.70E-15
P20810	ICAL	Calpastatin	↓3.18	0.0008
P24534	EF1B	Elongation factor 1-beta	↓3.16	3.46E-06
Q16778	H2B2E	Histone H2B type 2-E	↓3.15	5.52E-11
P10412	H14	Histone H1.4	↓3.13	7.54E-05
P63167	DYL1	Dynein light chain 1, cytoplasmic	↓3.12	2.55E-11
P08758	ANXA5	Annexin A5	↓3.10	0.0553
Q96TA1	NIBL1	Niban-like protein 1	↓3.02	1.69E-08
P60660	MYL6	Myosin light polypeptide 6	↓2.97	1.73E-07
P08865	RSSA	40S ribosomal protein SA	↓2.91	2.93E-13
Q00610	CLH1	Clathrin heavy chain 1	↓2.90	9.23E-09

TABLE 1 (Continued)

Accession number	Protein description	Protein symbol	Fold change	p value ^a
P0DP25	CALM3	Calmodulin-3	↓2.90	0.0010
P22528	SPR1B	Cornifin-B	↓2.81	0.0026
P60985	KTDAP	Keratinocyte differentiation-associated protein	↓2.76	4.26E-05
Q9Y6R7	FCGBP	IgGfC-binding protein	↓2.73	0.2858
P08238	HS90B	Heat shock protein HSP 90-beta	↓2.68	2.59E-09
Q9UHA7	IL36A	Interleukin-36 alpha	↓2.68	5.46E-10
Q14240	IF4A2	Eukaryotic initiation factor 4A-II	↓2.67	3.08E-10
Q6E0U4	DMKN	Dermokine	↓2.67	0.0012
P35321	SPR1A	Cornifin-A	↓2.65	0.0058
P29692	EF1D	Elongation factor 1-delta	↓2.65	1.95E-05
Q8NFU4	FDSCP	Follicular dendritic cell-secreted peptide	↓2.63	0.0014
Q14CN2	CLCA4	Calcium-activated chloride channel regulator 4	↓2.63	0.0004
Q06830	PRDX1	Peroxiredoxin-1	↓2.57	1.44E-13
Q96DA0	ZG16B	Zymogen granule protein 16 homolog B	↓2.53	0.0154
Q93077	H2A1C	Histone H2A type 1C	↓2.51	0.0002
Q96HE7	ERO1A	ERO1-like protein alpha	↓2.50	4.71E-13
P16152	CBR1	Carbonyl reductase [NADPH] 1	↓2.49	1.75E-08
P13797	PLST	Plastin-3	↓2.48	2.22E-12
P26641	EF1G	Elongation factor 1-gamma	↓2.46	5.75E-10
P06576	ATPB	ATP synthase subunit beta, mitochondrial	↓2.46	2.26E-09
P29373	RABP2	Cellular retinoic acid-binding protein 2	↓2.44	5.00E-07
Q16610	ECM1	Extracellular matrix protein 1	↓2.42	1.25E-07
A8K2U0	A2ML1	Alpha-2-macroglobulin-like protein 1	↓2.41	1.93E-08
Q8NHW5	RLA0L	60S acidic ribosomal protein P0-like	↓2.40	2.01E-09
Q9BTM1	H2AJ	Histone H2A.J	↓2.32	0.0013
P61978	HNRPK	Heterogeneous nuclear ribonucleoprotein K	↓2.27	2.17E-09
P04080	CYTB	Cystatin-B	↓2.26	4.65E-11
Q9BYE4	SPR2G	Small proline-rich protein 2G	↓2.25	0.0298
Q5VT79	AXA81	Annexin A8-like protein 1	↓2.21	0.0002
P13688	CEAM1	Carcinoembryonic antigen-related cell adhesion molecule 1	↓2.19	7.23E-05
P61026	RAB10	Ras-related protein Rab-10	↓2.17	4.69E-12
P30101	PDIA3	Protein disulfide-isomerase A3	↓2.15	7.71E-11
P15311	EZRI	Ezrin	↓2.11	2.92E-05
Q6ZN66	GBP6	Guanylate-binding protein 6	↓2.10	6.94E-06
Q9UJ70	NAGK	N-acetyl-D-glucosamine kinase	↓2.10	8.08E-11
Q9BQE3	TBA1C	Tubulin alpha-1C chain	↓2.10	1.04E-08
O75367	H2AY	Core histone macro-H2A.1	↓2.08	2.34E-08
P40199	CEAM6	Carcinoembryonic antigen-related cell adhesion molecule 6	↓2.08	0.0180
Q8TAX7	MUC7	Mucin-7	↓2.06	0.1305
P06753	TPM3	Tropomyosin alpha-3 chain	↓2.03	0.0067
P61604	CH10	10 kDa heat shock protein, mitochondrial	↓2.02	5.64E-06
P63104	1433Z	14-3-3 protein zeta/delta	↓2.01	4.14E-12
P50995	ANX11	Annexin A11	↓2.01	2.96E-09

Note: ↑Represents upregulation and ↓ Represents downregulation.

^aStudent's t-test.

interactions (PPIs). Hierarchical clustering of identified peptides based on the protein quantifications was represented with a heat map. In terms of prioritized proteins, individual whisker plots for each protein and volcanos plots of proteins were also generated. These plots were produced with GraphPad Prism 8.0 Software (La Jolla, CA, USA).

2.8 | Diagnostic yield

The normalized light/heavy area ratio of each peptide was extracted. Generalized regression models (GLMs) were then computerized in order to obtain candidate biomarkers. Initially, proteins detected in >50% of individuals in at least one group were selected. Secondly, proteins found significance among subgroups were prioritized. Thirdly, a GLM involving a protein panel was developed by means of machine learning particularly using the Wrapper-based forward feature-selection method. A panel of six proteins was prioritized based on this approach (MMP8, MMP9, A1BG, AACT, HBB, and HBD). Backward method was applied in order to improve GLMs fitness. A receiver-operating characteristic (ROC) analysis was then performed to plot the diagnostic yield. The threshold that maximized the function was used as the optimal cut-off point. The area under the curve (AUC), sensitivity, and specificity were then computerized by bootstrapping methods. For this aim, R software v.4.1.0 and pROC package were used.

3 | RESULTS

Group 1 comprised 18 patients (14 women and 4 men) with MRONJ. Mean age of the participants was 69.8 ± 9.5 . In terms of BMAs

prescribed, patients consumed intravenous zoledronate ($n = 12$), oral pamidronate ($n = 2$), and subcutaneous denosumab ($n = 4$). MRONJ cases also received BMAs treatment for a longer period (24.5 ± 18.1 months), on the other hand, BMAs consumer controls group for a reduced period of time (18.10 ± 10.97 months) reaching no significance ($p = .29$). The most common stage was stage 1 with 15 (83.3%) cases followed by 2 cases in stage 2 (11.1%) and 1 stage 3 case (6.6%). In 13 cases MRONJ was located on the mandible. The most common local risk factors were dental extraction ($n = 10$) and periodontitis treatment ($n = 2$). Although six cases developed spontaneously. Pain was a symptom in 3 MRONJ cases with all exhibiting evidence of infection in the form of an intraoral fistula, one case presented an extraoral fistula. The case groups were composed of 20 participants (10 per group). Group 2 of 68.9 and the Group 3 of 71.8 years of age.

The results of the intraoral examination of the three study groups are shown in (Table S1, Appendix p. 1). There were no significant differences among groups in terms of primary diseases (Table S2, Appendix p. 2). Other possible confounders such as corticosteroid treatment, chemotherapy, or tobacco use did not differ among groups ($p > .05$).

SWATH analysis allowed the identification of 586 proteins. The information obtained in this library about the retention time, MS, and MSMS of all peptides in all proteins were used to perform a SWATH analysis. As aforementioned PCA and OPLS-DA were carried out to normalized data. PC1 and PC2 components could explain the 68.0% and 9.7%, respectively, of data variability between groups.

A total of three comparisons were made between MRONJ and the two groups: (I) both control groups versus MRONJ, (II) controls

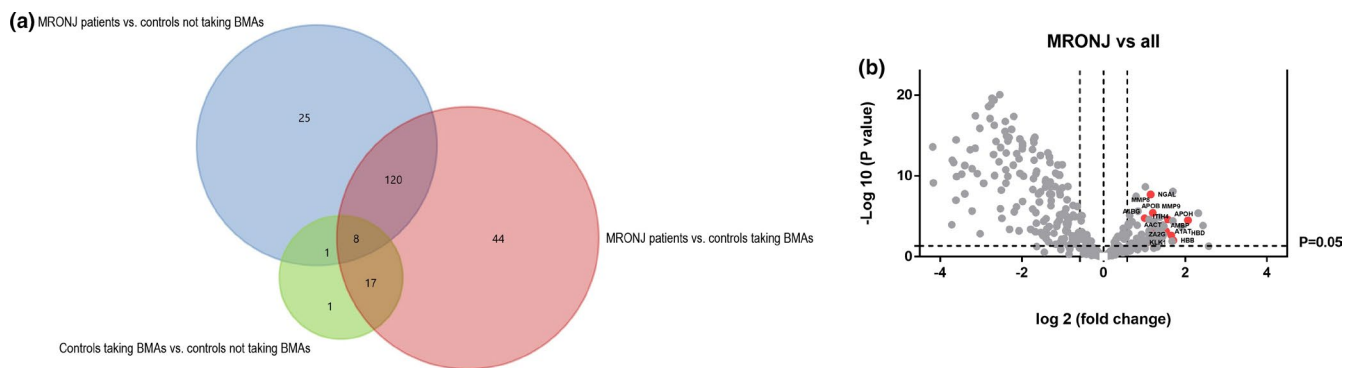
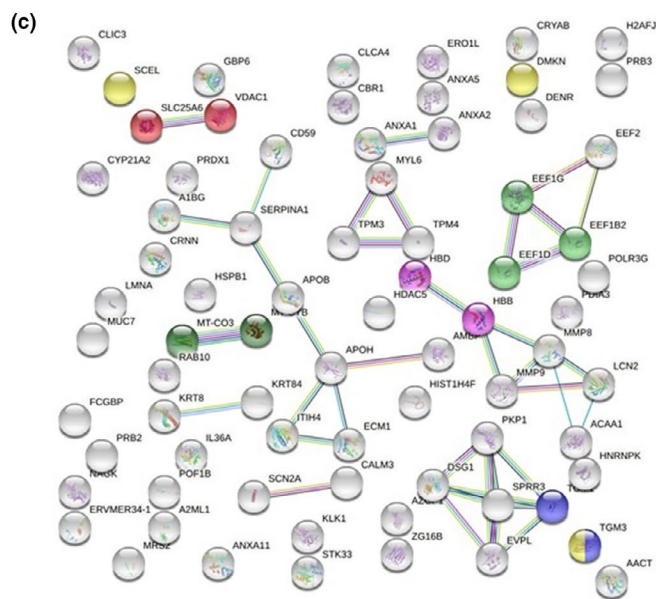
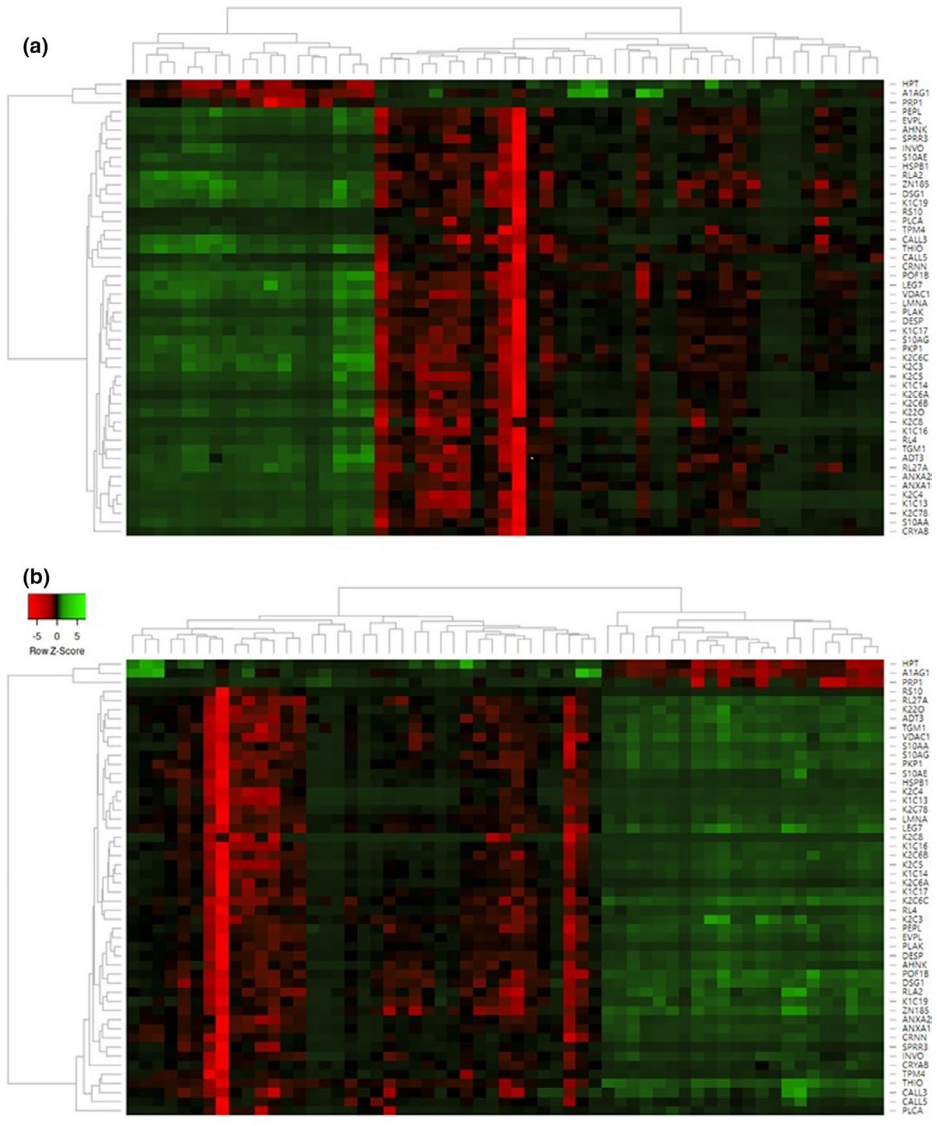


FIGURE 2 (a) Venn diagram displaying the differentially expressed proteins ($p < .05/FC \geq 2$) and overlaps across the three groups by use of quantitative proteomics. (b) Volcano diagram delineating the comparison of MRONJ group and both control groups. Proteins were separated on the basis of the \log_2 of the FC (x-axis) and the $-\log_{10}$ of the p -values based on t-test (y-axis). The clusters of prioritized proteins were named and marked as red bubbles

FIGURE 3 (a) Heat map of proteins significantly up and down expressed between the MRONJ and control group 1. (b) Heat map of proteins significantly upregulated and downregulated between the MRONJ and control group 2. Only significantly different expressed proteins are represented (≥ 2 fold and p value $< .05$). Columns represent each saliva sample and rows the individual proteins. Protein intensities of expression were \log_{10} -transformed and displayed as colors from red to green. Clustering separating samples into three predefined subgroups. (c) Protein-protein interaction network of proteins according to STRING



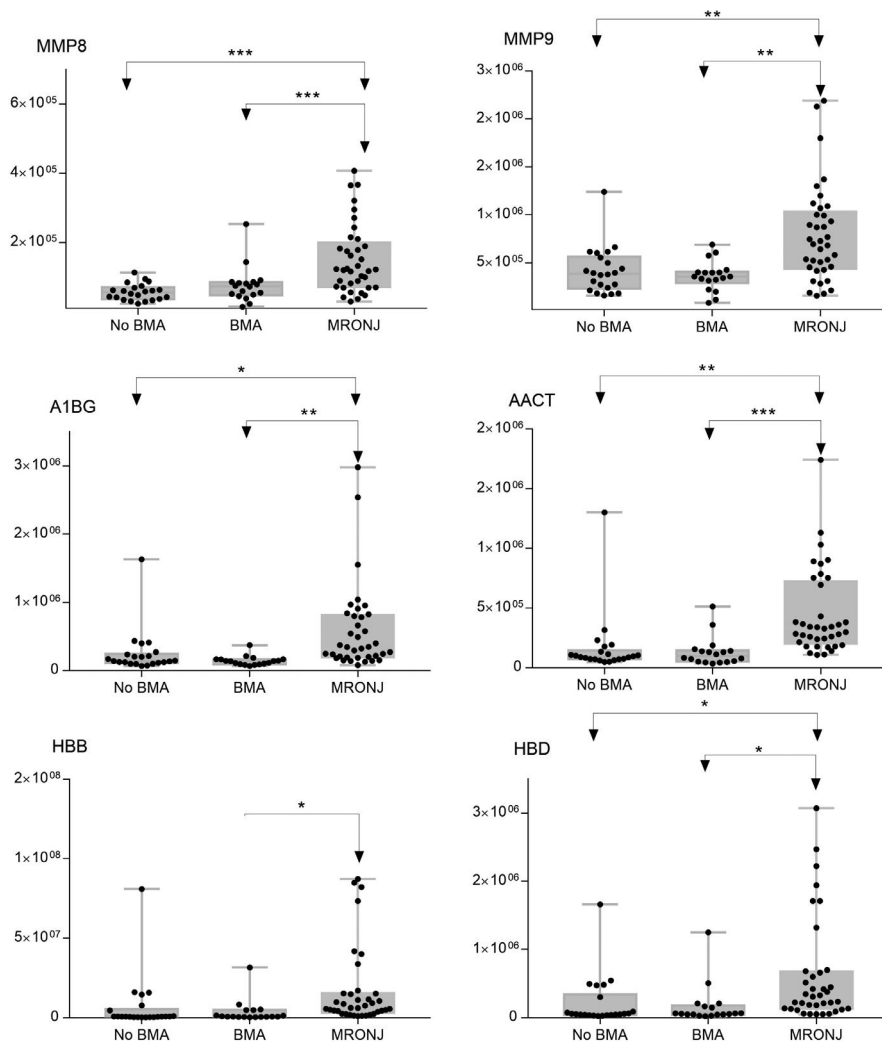


FIGURE 4 Whisker plot visualization of percent change based on DIA quantification. Boxes show the saliva concentration changes of MMP8, MMP9, A1BG, AACT, HBB, and HBD in each of the three subgroups. The protein expression of each sample is plotted. The upper error bars signify the 90th percentile, and lower error bars represent the 10th percentile while the middle line accounts for the median. Open squares represent the mean protein abundance and its respective significance (* $p < .05$, ** $p < .01$, *** $p < .001$)

taking BMAs versus MRONJ, and III) controls not consuming BMAs versus MRONJ. In comparison I, 175 proteins were differentially expressed ($p < .05$) in MRONJ versus both control groups, these data are shown in Table 1. Differential expression is displayed in a Venn diagram representing comparisons II and III (Figure 2a). Tables S3 and S4 (Appendix p. 3-15) show the upregulated and downregulated proteins in comparisons II and III, respectively. Volcano plot of proteins significantly regulated between three groups with an FC above 2 is displayed in Figure 2b. Attention was drawn to the upregulated proteins in comparison I. Identified proteome was divided into three hubs. The first group of included proteins was relevant for the maintenance of extracellular matrix and protease binding (i.e., LCN2, MMP8, and MMP9). The second group comprised proteins involved in the acute-phase response, platelet degranulation, and triglyceride metabolic process (i.e., A1BG, AACT, AMBP, APOB, APOH, AZGP1, ITIH4, KLK1, and SERPINA1). The final cluster plays a role in oxygen transport (i.e., HBB, HBD, and SCN2A). Proteins belonging to these hubs were marked with red (Figure 2b).

After statistical analysis, a heat map cluster analysis was performed. The unsupervised hierarchical clustering analysis clearly discriminated between the three groups of samples in comparisons II/III (Figure 3a,b). STRING app was used to characterize the PPIs

comparison I. The resulting network was composed of 75 nodes (proteins) and 39 edges (interactions) (Figure 3b). Only 34 proteins that showed no interactions with other proteins in comparison I (Figure 3c). The p value of PPI enrichment was 1.41×10^{-10} , while the clustering coefficient was 0.409. Regarding biological processes, the most involved were cell envelope organization, positive regulation of vesicle fusion, positive regulation of receptor binding, and the regulation of low-density lipoprotein particle clearance. Regarding molecular functions, identified proteins were enriched in phospholipase A2 inhibitor activity, phospholipase inhibitor activity, translation elongation factor activity, protein-glutamine gamma-glutamyltransferase activity, and calcium channel inhibitor activity.

Potential protein biomarkers (MMP8, MMP9, A1BG, AACT, HBB, and HBD) abundance was normalized to the total protein abundance as displayed in whisker plots. All selected proteins were upregulated in MRONJ (Figure 4). The model was subjected to a process of optimization. In this process, 3 proteins were selected for a panel (MMP9, AACT, and HBD). ROC analysis was then performed. The AUC for differentiating between MRONJ and controls was 0.879 with a sensitivity of 90% and a specificity of 78.9% (Figure 5).

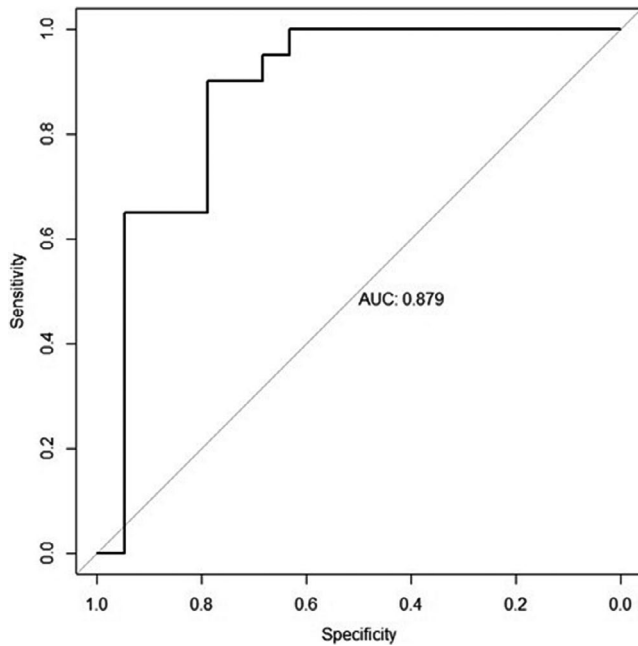


FIGURE 5 Receiver-operating characteristic curve of three proteins model using for differentiating between participants with medication-related osteonecrosis of the jaw both and control groups. AUC, area under the curve

4 | DISCUSSION

To date, scientific literature has failed to demonstrate reliable biomarkers to predict or establish a prognosis for MRONJ (Lorenzo-Pouso et al., 2019). Works described in the literature addressing this issue have mainly used serum as an analytical matrix. In this regard, bone-related and endocrine biomarkers are the most discussed in the literature, including CTX, NTX, BAP, PTH, or NF- κ B ligand (Bagan et al., 2014; Bagan et al., 2008; Bagan et al., 2017; Kim et al., 2013).

Mechanistic insights into the involved salivary protein fingerprints, networks, and processes that may precipitate the onset of MRONJ remain elusive (Otto et al., 2018). We have demonstrated that discriminatory proteomic biomarkers are present in human saliva when MRONJ developed. To the best of our knowledge, this is the first study to use a comprehensive high-throughput quantitative proteomic technique, supported by a bioinformatics analysis involving process network and GO process enrichment tools, to discover salivary biomarkers in MRONJ.

Through SWATH-MS, 586 proteins were quantitatively identified from saliva in the present study. This study ascertained that 123 proteins were consistently downregulated, while 52 proteins were upregulated in comparison I. Most of these proteins are related to the current MRONJ etiology model based on three mainstays: (i) inhibition of osteoclastic bone resorption/remodeling, (ii) inflammation/infection, and (iii) angiogenesis inhibition (Aghaloo et al., 2015).

As a preliminary step, we examined three main clusters, and the prioritized 6 proteins upregulated in MRONJ. The first was related

to the extracellular matrix and protease binding. MMPs play a pivotal role in the degradation/remodeling of the extracellular matrix (Rawlings & Barrett, 1995). Bacterial components enhance macrophage and lymphocyte activity resulting in the production of inflammatory mediators and ultimately MMPs delivery by fibroblast (Zhang et al., 2013). Among all the MMPs identified in our study, we put the focus on MMP8 and MMP9.

MMP9 is the major liable enzyme in active periodontal tissue destruction. Increased expression of MMP8 also promotes osteoclast differentiation and activity (Sorsa et al., 2004). Little data are currently available showing that periodontitis is an independent MRONJ risk factor (Thumbigere-Math et al., 2014; Vahtsevanos et al., 2009). Nonetheless, a recent pooled analysis performed demonstrated that the prevalence of periodontitis was significantly higher in MRONJ (Lorenzo-Pouso et al., 2020). Therefore, this protein upregulation reinforces a plausible link with periodontitis.

MMP8 is a zinc-dependent endopeptidase that degrades collagen, and its production is mainly based on macrophages and granulocytes (Sorsa et al., 2004). Expression of MMP8 has been recently associated with some diseases, including cancer (Huang, 2018). Basi et al. demonstrated via a mouse model that zoledronate can increase MMP9 activity due to RANKL expression (Basi et al., 2011). Thumbigere-Math et al. also identified an overexpression of this protein in the saliva of MRONJ patients (Thumbigere-Math et al., 2015). Nonetheless, they did not include the group of healthy patients. In this vein, they hypothesized that cancer may act as a confounder. Here, we can ensure that MMP9 is considerably overexpressed in MRONJ, and cancer does not introduce selection bias.

Proteins rarely perform a biological function independently. Therefore, we analyzed MMP PPIs (Figure 2). Among the MMPs interacting proteins, we highlight LCN2. LCN2 protects MMPs from proteolysis (Bolignano et al., 2008). It has been hypothesized that LCN2 enhances MMP8 and MMP9 activity complex via lipid metabolism and intravascular coagulation (Otto et al., 2010).

The second cluster was mainly built by proteins involved in the acute-phase response, platelet degranulation, and triglyceride metabolic process. Among them, A1BG and AACT were prioritized owed to terms previously described. It has been reported that TNF blocking treatments resulted in A1BG overexpression and inflammation mitigation (Estelius et al., 2019). AACT inhibits the activity of proteases, such as cathepsin G. It has been proven that Cathepsin G activates other proteolytic cascades that trigger neutrophil collagenase activity (Korkmaz et al., 2010).

Final cluster is related to oxygen transport. HDB and HDD are proteins in specialized O₂-transport acting on aerobic metabolism. Due to the multiple molecular transport across salivary acini and blood vessel endothelium cells, the upregulated presence of these clusters mirrors efforts in circulation to mitigate MRONJ (Marx, 2003).

This case-control study has several limitations. Laboratory tests of any kind of potential biomarker as a risk predictor would be more useful when conducted before the exposure to a relevant

risk factor such as dentoalveolar surgery, rather than once MRONJ is established. This timing is a limitation of this research. Despite our attempts to balance cases and controls on the basis of BMAs exposure, treatment duration significantly differed between MRONJ cases and controls.

To conclude, the current findings open a new venue for these proteins to serve in revealing the molecular underpinnings of MRONJ. Further studies are needed to ascertain whether identified biomarkers may be useful.


AUTHOR CONTRIBUTIONS

Conceptualization; Data curation; Formal analysis; Funding acquisition; Investigation; Methodology; Project administration; Resources; Software; Supervision; Validation; Visualization; Writing – original draft: Alejandro I. Lorenzo-Pouso. Conceptualization; Data curation; Formal analysis; Funding acquisition; Investigation; Methodology; Project administration; Resources; Software; Supervision; Validation; Visualization; Writing – review & editing: Javier Carballo. Data curation; Formal analysis; Investigation; Supervision; Validation: Maria del Pilar Chantada-Vázquez. Conceptualization; Data curation; Formal analysis; Funding acquisition; Investigation; Methodology; Project administration; Resources; Supervision; Validation; Visualization; Writing – review & editing: Jose Bagan. Investigation; Methodology; Visualization: Leticia Bagán. Data curation; Formal analysis; Investigation; Software; Supervision; Validation; Visualization: Cintia Chamorro. Formal analysis; Software; Supervision; Validation: Mercedes Conde-Amboage. Conceptualization; Data curation; Project administration; Visualization; Writing – review & editing: Rafael López-López. Conceptualization; Data curation; Project administration; Resources; Supervision; Validation; Visualization; Writing – review & editing: Abel García. Conceptualization; Data curation; Investigation; Methodology; Resources; Supervision; Validation; Visualization; Writing – original draft; Writing – review & editing: M Perez-Sayans.

PEER REVIEW

The peer review history for this article is available at <https://publons.com/publon/10.1111/odi.14201>.

ORCID

Alejandro I. Lorenzo-Pouso  <https://orcid.org/0000-0002-9180-4703>

Cintia M. Chamorro-Petronacci  <https://orcid.org/0000-0002-5637-9908>

Mario Pérez-Sayáns  <https://orcid.org/0000-0003-2196-9868>

REFERENCES

- Aghaloo, T., Hazboun, R., & Tetradis, S. (2015). Pathophysiology of osteonecrosis of the jaws. *Oral and Maxillofacial Surgery Clinics of North America*, 27(4), 489–496. <https://doi.org/10.1016/j.coms.2015.06.001>
- Bagan, J. V., Jimenez, Y., Gomez, D., Sirera, R., Poveda, R., & Scully, C. (2008). Collagen telopeptide (serum CTX) and its relationship with the size and number of lesions in osteonecrosis of the jaws in cancer patients on intravenous bisphosphonates. *Oral Oncology*, 44(11), 1088–1089. <https://doi.org/10.1016/j.oraloncology.2008.01.012>
- Bagan, J., Sáez, G. T., Tormos, M. C., Gavalda-Esteve, C., Bagan, L., Leopoldo-Rodado, M., Calvo, J., & Camps, C. (2014). Oxidative stress in bisphosphonate-related osteonecrosis of the jaws. *Journal of Oral Pathology & Medicine*, 43(5), 371–377. <https://doi.org/10.1111/jop.12151>
- Bagan, J., Sáez, G. T., Tormos, M. C., Hens, E., Terol, M. J., Bagan, L., Diaz-Fernández, J. M., Lluch, A., & Camps, C. (2014). Interleukin-6 concentration changes in plasma and saliva in bisphosphonate-related osteonecrosis of the jaws. *Oral Diseases*, 20(5), 446–452. <https://doi.org/10.1111/odi.12150>
- Bagan, J., Sheth, C. C., Soria, J. M., Margaix, M., & Bagan, L. (2013). Bisphosphonates-related osteonecrosis of the jaws: A preliminary study of salivary interleukins. *Journal of Oral Pathology & Medicine*, 42(5), 405–408. <https://doi.org/10.1111/jop.12021>
- Bagan, L., Jimenez, Y., Leopoldo, M., Rubert, A., & Bagan, J. (2017). Serum levels of RANKL and OPG, and the RANKL/OPG ratio in bisphosphonate-related osteonecrosis of the jaw: Are they useful biomarkers for the advanced stages of osteonecrosis? *Medicina Oral Y Cirugia Bucal*, 22(5), e542–e547. <https://doi.org/10.4317/medoral.22128>
- Basi, D. L., Hughes, P. J., Thumbigere-Math, V., Sabino, M., Mariash, A., Lunos, S. A., Jensen, E., & Gopalakrishnan, R. (2011). Matrix metalloproteinase-9 expression in alveolar extraction sockets of zoledronic acid-treated rats. *Journal of Oral and Maxillofacial Surgery*, 69(11), 2698–2707. <https://doi.org/10.1016/j.joms.2011.02.065>
- Bateman, N. W., Goulding, S. P., Shulman, N. J., Gadok, A. K., Szumlinski, K. K., MacCoss, M. J., & Wu, C. C. (2014). Maximizing peptide identification events in proteomic workflows using data-dependent acquisition (DDA). *Molecular & Cellular Proteomics: MCP*, 13(1), 329–338. <https://doi.org/10.1074/mcp.M112.026500>
- Bolignano, D., Donato, V., Coppolino, G., Campo, S., Buemi, A., Lacquaniti, A., & Buemi, M. (2008). Neutrophil gelatinase-associated lipocalin (NGAL) as a marker of kidney damage. *American Journal of Kidney Diseases*, 52(3), 595–605. <https://doi.org/10.1053/ajkd.2008.01.020>
- Chantada-Vázquez, M. P., López, A. C., Vence, M. G., Vázquez-Estévez, S., Acea-Nebri, B., Calatayud, D. G., Jardiel, T., Bravo, S. B., & Núñez, C. (2020). Proteomic investigation on bio-corona of Au, Ag and Fe nanoparticles for the discovery of triple negative breast cancer serum protein biomarkers. *Journal of Proteomics*, 212, e103581. <https://doi.org/10.1016/j.jprot.2019.103581>
- Estelius, J., Lengqvist, J., Ossipova, E., Idborg, H., Le Maître, E., Andersson, M. L. A., Brundin, L., Khademi, M., Svenungsson, E., Jakobsson, P.-J., & Lampa, J. (2019). Mass spectrometry-based analysis of cerebrospinal fluid from arthritis patients-immune-related candidate proteins affected by TNF blocking treatment. *Arthritis Research & Therapy*, 21(1), 60–66. <https://doi.org/10.1186/s13075-019-1846-6>
- Huang, H. (2018). Matrix metalloproteinase-9 (MMP-9) as a cancer biomarker and MMP-9 biosensors: Recent advances. *Sensors (Basel, Switzerland)*, 18(10), e3249. <https://doi.org/10.3390/s18103249>
- Kim, J. W., Kong, K. A., Kim, S. J., Choi, S. K., Cha, I. H., & Kim, M. R. (2013). Prospective biomarker evaluation in patients with osteonecrosis of the jaw who received bisphosphonates. *Bone*, 57(1), 201–205. <https://doi.org/10.1016/j.bone.2013.08.005>
- Korkmaz, B., Horwitz, M. S., Jenne, D. E., & Gauthier, F. (2010). Neutrophil elastase, proteinase 3, and cathepsin G as therapeutic targets in human diseases. *Pharmacological Reviews*, 62(4), 726–759. <https://doi.org/10.1124/pr.110.002733>
- Lorenzo-Pouso, A. I., Pérez-Sayáns, M., Chamorro-Petronacci, C., Gándara-Vila, P., López-Jornet, P., Carballo, J., & García-García, A. (2020). Association between periodontitis and medication-related osteonecrosis of the jaw: A systematic review and meta-analysis.

- Journal of Oral Pathology & Medicine*, 49(3), 190–200. <https://doi.org/10.1111/jop.12963>
- Lorenzo-Pouso, A. I., Perez-Sayans, M., Gonzalez-Palanca, S., Chamorro-Petronacci, C., Bagan, J., & Garcia-Garcia, A. (2019). Biomarkers to predict the onset of bisphosphonate-related osteonecrosis of the jaw: A systematic review. *Medicina Oral, Patologia Oral Y Cirugia Bucal*, 24(1), e26–e36. <https://doi.org/10.4317/medoral.22763>
- Marx, R. E. (2003). Pamidronate (aredia) and zoledronate (zometa) induced avascular necrosis of the jaws: A growing epidemic. *Journal of Oral and Maxillofacial Surgery*, 61(9), 1115–1117. [https://doi.org/10.1016/s0278-2391\(03\)00720-1](https://doi.org/10.1016/s0278-2391(03)00720-1)
- Otto, S., Hafner, S., Mast, G., Tischer, T., Volkmer, E., Schieker, M., Stürzenbaum, S. R., von Tresckow, E., Kolk, A., Ehrenfeld, M., & Pautke, C. (2010). Bisphosphonate-related osteonecrosis of the jaw: Is pH the missing part in the pathogenesis puzzle? *Journal of Oral and Maxillofacial Surgery*, 68(5), 1158–1161. <https://doi.org/10.1016/j.joms.2009.07.079>
- Otto, S., Pautke, C., Van den Wyngaert, T., Niepel, D., & Schiodt, M. (2018). Medication-related osteonecrosis of the jaw: Prevention, diagnosis and management in patients with cancer and bone metastases. *Cancer Treatment Reviews*, 69, 177–187. <https://doi.org/10.1016/j.ctrv.2018.06.007>
- Rawlings, N. D., & Barrett, A. J. (1995). Evolutionary families of metalloproteinases. *Methods in Enzymology*, 248, 183–228. [https://doi.org/10.1016/0076-6879\(95\)48015-3](https://doi.org/10.1016/0076-6879(95)48015-3)
- Reid, I. R. (2015). Efficacy, effectiveness and side effects of medications used to prevent fractures. *Journal of Internal Medicine*, 277(6), 690–706. <https://doi.org/10.1111/joim.12339>
- Rifai, N., Gillette, M. A., & Carr, S. A. (2006). Protein biomarker discovery and validation: The long and uncertain path to clinical utility. *Nature Biotechnology*, 24(8), 971–983. <https://doi.org/10.1038/nbt1235>
- Ruggiero, S. L., Dodson, T. B., Fantasia, J., Goodday, R., Aghaloo, T., Mehrotra, B., & O’Ryan, F. (2014). American association of oral and maxillofacial surgeons position paper on medication-related osteonecrosis of the jaw—2014 update. *Journal of Oral and Maxillofacial Surgery*, 72(10), 1938–1956. <https://doi.org/10.1016/j.joms.2014.04.031>
- Schiodt, M., Otto, S., Fedele, S., Bedogni, A., Nicolatou-Galitis, O., Guggenberger, R., Herlofson, B. B., Ristow, O., & Kofod, T. (2019). Workshop of European task force on medication-related osteonecrosis of the jaw-current challenges. *Oral Diseases*, 25(7), 1815–1821. <https://doi.org/10.1111/odi.13160>
- Sorsa, T., Tjaderhane, L., & Salo, T. (2004). Matrix metalloproteinases (MMPs) in oral diseases. *Oral Diseases*, 10(6), 311–318. <https://doi.org/10.1111/j.1601-0825.2004.01038.x>
- Thumbigere-Math, V., Michalowicz, B. S., Hodges, J. S., Tsai, M. L., Swenson, K. K., Rockwell, L., & Gopalakrishnan, R. (2014). Periodontal disease as a risk factor for bisphosphonate-related osteonecrosis of the jaw. *Journal of Periodontology*, 85(2), 226–233. <https://doi.org/10.1902/jop.2013.130017>
- Thumbigere-Math, V., Michalowicz, B. S., Jong, E. P., Griffin, T. J., Basi, D. L., Hughes, P. J., Tsai, M. L., Swenson, K. K., Rockwell, L., & Gopalakrishnan, R. (2015). Salivary proteomics in bisphosphonate-related osteonecrosis of the jaw. *Oral Diseases*, 21(1), 46–56. <https://doi.org/10.1111/odi.12204>
- Vahntsevanos, K., Kyrgidis, A., Verrou, E., Katodritou, E., Triaridis, S., Andreadis, C. G., Boukovinas, I., Koloutsos, G. E., Teleioudis, Z., Kitikidou, K., Paraskevopoulos, P., Zervas, K., & Antoniadis, K. (2009). Longitudinal cohort study of risk factors in cancer patients of bisphosphonate-related osteonecrosis of the jaw. *Journal of Clinical Oncology*, 27(32), 5356–5362. <https://doi.org/10.1200/JCO.2009.21.9584>
- von Elm, E., Altman, D. G., Egger, M., Pocock, S. J., Gøtzsche, P. C., Vandenbroucke, J. P. (2008). The strengthening the reporting of observational studies in epidemiology (STROBE) statement: Guidelines for reporting observational studies. *Journal of Clinical Epidemiology*, 61(4), 344–349. <https://doi.org/10.1016/j.jclinepi.2007.11.008>
- Zhang, Q., Atsuta, I., Liu, S., Chen, C., Shi, S., Shi, S., & Le, A. D. (2013). IL-17-mediated M1/M2 macrophage alteration contributes to pathogenesis of bisphosphonate-related osteonecrosis of the jaws. *Clinical Cancer Research*, 19(12), 3176–3188. <https://doi.org/10.1158/1078-0432.CCR-13-0042>

SUPPORTING INFORMATION

Additional supporting information may be found in the online version of the article at the publisher’s website.

How to cite this article: Lorenzo-Pouso, A. I., Bravo, S. B., Carballo, J., del Chantada-Vázquez, M. P., Bagán, J., Bagán, L., Chamorro-Petronacci, C. M., Conde-Amboage, M., López-López, R., García-García, A., & Pérez-Sayáns, M. (2022). Quantitative proteomics in medication-related osteonecrosis of the jaw: A proof-of-concept study. *Oral Diseases*, 00, 1–13. <https://doi.org/10.1111/odi.14201>